International Journal of Modern Physics E
Vol. 24, No. 3 (2015) 1550017 (17 pages)

DOI: 10.1142/S0218301315500172

Shape coexistence and parity doublet in Zr isotopes

Bharat Kumar*, S. K. Singh and S. K. Patra

Institute of Physics
Bhubaneswar 751 005, India
**bharat@iopb.res.in*

Received 11 September 2014
Revised 26 January 2015
Accepted 8 February 2015
Published 17 March 2015

The ground and excited states properties of Zr isotopes are studied from proton to neutron drip lines using the relativistic (RMF) and nonrelativistic (SHF) mean-field formalisms with Bardeen–Cooper–Schrieffer (BCS) and Bogoliubov pairing, respectively. The well-known NL3* and SLy4 parameter sets are used in the calculations. We have found spherical ground and low-lying large deformed excited states in most of the isotopes. Several couples of $\Omega^{\pi} = 1/2^{\pm}$ parity doublets configurations are noticed, while analyzing the single-particle energy levels of the large deformed configurations.

Keywords: Relativistic mean-field theory; Skyrme–Hartree–Fock–Bogoliubov theory; parity doublet; shape coexistence.

PACS Number(s): 21.10.Dr, 21.10.Hw, 21.10.Ft, 21.10.Pc

1. Introduction

Although nuclear shape coexistence in various mass regions of the periodic table is well-known, it remains an interesting investigation till today. On the other hand, the existence of parity doublet is relatively new.[1–3] The origin and manifestation of such an interesting observable is not yet known clearly. It is reported that the parity doublet is not visible in a nucleus with normal/spherical deformation. However, the existence of parity doublet is possible for nuclei with highly deformed shape. In this case, two orbitals with opposite parity lie very close to each other. Since, the parity doublets only appear in large deformed configuration and not in normal or spherical shape, its origin may be related to its shape, i.e., with deformed orbitals. That means, in normal situation, the high-lying partner of the doublet does not come nearer to the low-lying one but when the nucleus gets deformed, gives rise a Nilsson like structure in the large deformed state. The shape coexistence, i.e., two different shapes very close in energy is also rare, but known in nuclear structure

*Corresponding author.

physics.[4–8] In this case, both the solutions are nearly or completely degenerate (different configuration with same energy). This phenomenon is mostly visible in the mass region $A = 100$ of the periodic table.[9] Here, we have chosen Zr nucleus as a potential candidate both for shape coexistence and study of parity doublets using the well known relativistic (RMF) and nonrelativistic (SHF) mean-field formalisms. The NL3* and SLy4 parametrization with Bardeen–Cooper–Schrieffer (BCS) and Bogoliubov pairing prescriptions, respectively used to take care of the pairing for the open shell nuclei. The paper is organized as follows: In Secs. 2 and 3, we have given a brief outline about the nonrelativistic Skyrme–Hartree–Fock–Bogoliubov (SHFB) and relativistic mean-field (RMF) formalisms. Our results are discussed in Sec. 4. A concluding remark is given in Sec. 5.

2. SHFB Approximation

The energy density functional with SHFB approximation is a powerful theoretical formalism to deal with finite nuclei starting from both proton to neutron drip lines.[10] In this calculations, we have used the successful SLy4 parameter set[11] with zero-range Bogoliubov pairing interaction for open shell nuclei. The numerical calculations are done using an axially deformed harmonic oscillator (HO) basis state expansion to solve the Schrödinger equation iteratively. The numerical calculations are carried out using the code HFBTHO (v1.66p)[12] that solve the equation self-consistently. For Skyrme forces, the Hartree–Fock–Bogoliubov (HFB) energy has the form of a local energy density functional[15–18]:

$$E[\rho, \tilde{\rho}] = \int d^3\mathbf{r}\mathcal{H}(\mathbf{r}), \tag{1}$$

where Hamiltonian density $\mathcal{H}$:

$$\mathcal{H}(\mathbf{r}) = H(\mathbf{r}) + \tilde{H}(\mathbf{r}), \tag{2}$$

is the sum of the mean-field and pairing energy densities. In the present implementation, we have used the following explicit forms:

$$\begin{aligned} H(\mathbf{r}) = {} & \frac{\hbar^2}{2m}\tau + \frac{1}{2}t_0\left[\left(1+\frac{1}{2}x_0\right)\rho^2 - \left(\frac{1}{2}+x_0\right)\sum_q \rho_q^2\right] \\ & + \frac{1}{2}t_1\left[\left(1+\frac{1}{2}x_1\right)\rho\left(\tau - \frac{3}{4}\Delta\rho\right)\right] - \left(\frac{1}{2}+x_1\right)\sum_q \rho_q\left(\tau_q - \frac{3}{4}\Delta\rho_q\right)\Bigg] \\ & + \frac{1}{2}t_2\left[\left(1+\frac{1}{2}x_2\right)\rho\left(\tau + \frac{1}{4}\Delta\rho\right) - \left(\frac{1}{2}+x_2\right)\sum_q \rho_q\left(\tau_q + \frac{1}{4}\Delta\rho_q\right)\right] \\ & + \frac{1}{12}t_3\rho^\alpha\left[\left(1+\frac{1}{2}x_3\right)\rho^2 - \left(x_3+\frac{1}{2}\right)\sum_q \rho_q^2\right] \end{aligned}$$

$$-\frac{1}{8}(t_1x_1+t_2x_2)\sum_{ij}\mathbf{J}_{ij}^2+\frac{1}{8}(t_1-t_2)\sum_{q,ij}\mathbf{J}_{q,ij}^2$$
$$-\frac{1}{2}W_0\sum_{ijk}\varepsilon_{ijk}\left[\rho\nabla_k\mathbf{J}_{ij}+\sum_q\rho_q\nabla_k\mathbf{J}_{q,ij}\right], \tag{3}$$

$$\tilde{H}(\mathbf{r})=\frac{1}{2}V_0\left[1-V_1\left(\frac{\rho}{\rho_0}\right)^{\gamma}\right]\sum_q\tilde{\rho}_q^2. \tag{4}$$

The index q labels is represents the neutron ($q=n$) or proton ($q=p$) densities, while densities without index q denote the sums of proton and neutron densities. $H(\mathbf{r})$ and $\tilde{H}(\mathbf{r})$ depend on the particle local density $\rho(\mathbf{r})$, pairing local density $\tilde{\rho}(\mathbf{r})$, kinetic energy density $\tau(\mathbf{r})$ and spin-current density $\mathbf{J}_{ij}(\mathbf{r})$. The number of oscillator shells $N_{\rm sh}=20$ and basis parameter $b_0=\sqrt{b_z^2+b_\perp^2}$ are used in the calculations. A detail numerical technique is available in Ref. 12 and the notations have their usual meaning.

2.1. *Pairing correlations in SHF formalism*

In nonrelativistic SHFB formalism, the pairing correlation is included by Lipkin–Nogami (LN) prescription.[12,13] Here, the LN method has been implemented by perturbing the SHFB calculation with an additional term $h'=h-2\lambda_2(1-2\rho)$ included in the Hartree–Fock (HF) Hamiltonian, where the parameter λ_2 is iteratively calculated to describe the curvature of the total energy as a function of the particle number. For an arbitrary two-body interaction $\hat{V}$, λ_2 can be calculated from the particle number dispersion according to the following relation[12]:

$$\lambda_2=\frac{\langle 0|\hat{V}|4\rangle\langle 4|\hat{N}^2|0\rangle}{\langle 0|\hat{N}^2|4\rangle\langle 4|\hat{N}^2|0\rangle}, \tag{5}$$

where $|0\rangle$ is the quasi-particle vacuum, $\hat{N}$ is the particle number operator, and $|4\rangle\langle 4|$ is the projection operator onto the four-quasi-particle operator space. The final expression for the λ_2 can be written in the following simple form[14]:

$$\lambda_2=\frac{1}{2}\frac{{\rm Tr}\Gamma'\rho(1-\rho)+{\rm Tr}\Delta'(1-\rho)\kappa}{[{\rm Tr}\rho(1-\rho)]^2-2{\rm Tr}\rho^2(1-\rho)^2}, \tag{6}$$

where κ is the pairing tensor and the potentials are given as

$$\Gamma'_{\alpha\alpha'}=\sum_{\beta\beta'}V_{\alpha\beta\alpha'\beta'}(\rho(1-\rho))_{\beta'\beta} \tag{7}$$

and

$$\Delta'_{\alpha\beta}=\frac{1}{2}\sum_{\alpha'\beta'}V_{\alpha\beta\alpha'\beta'}(\rho\kappa)_{\alpha'\beta'}, \tag{8}$$

which can be calculated in a full analogy to Γ and Δ by replacing ρ and κ by $\rho(1-\rho)$ and $\rho\kappa$, respectively. In case of the seniority pairing interaction with strength G,

Eq. (6) can be simplified to

$$\lambda_2 = \frac{G}{4}\frac{\mathrm{Tr}(1-\rho)\kappa\,\mathrm{Tr}\rho\kappa - 2\,\mathrm{Tr}(1-\rho)^2\rho^2}{[\mathrm{Tr}\,\rho(1-\rho)]^2 - 2\,\mathrm{Tr}\rho^2(1-\rho)^2}. \tag{9}$$

Equation (6) can be well approximated by the seniority pairing expression (9) with the effective strength (G) and can be written in terms of pairing energy (E_{pair}) and average pairing gap ($\bar{\Delta}$)[12]:

$$G = G_{\mathrm{eff}} = -\frac{\bar{\Delta}^2}{E_{\mathrm{pair}}}, \tag{10}$$

where, $E_{\mathrm{pair}} = -\frac{1}{2}\mathrm{Tr}\Delta\kappa$ and $\bar{\Delta} = \frac{\mathrm{Tr}\Delta\rho}{\mathrm{Tr}\rho}$.

The calculation is done using the density-dependent delta pairing force with the pairing strength $V_0 = -244.72\,\mathrm{MeV\,fm^3}$, and pairing window 60 MeV. These quantities have been fitted to reproduce the neutron pairing gap of ^{120}Sn which is consistent with Ref. 19. Average pairing gap ($\bar{\Delta}$) is obtained from the level density. Thus, it varies from nucleus to nucleus depending on the density distribution of nucleons. The results for pairing gaps ($\triangle_n$, $\triangle_p$), effective strength (G_n, G_p) and pairing energy (E_{pair}) for Zr isotopes are given in Table 1.

3. Theoretical Framework for RMF Model

The RMF model[20–25] is largely used in recent years for both finite nuclei and infinite nuclear matter from normal to supernormal conditions. We have used the RMF Lagrangian[24] with the NL3* parameter set,[26] which is reasonably useful for both β-stable and drip lines nuclei. The Lagrangian contains the terms of interaction between mesons and nucleons and also self-interaction of isoscalar scalar *sigma* meson. The other mesons are isoscalar vector *omega* and isovector vector *rho* mesons. The photon field A_μ is included to take care of the Coulombic interaction of protons. A definite set of coupled equations are obtained from the Lagrangian which are solved self-consistently in an axially deformed HO basis with $N_F = N_B = 12$, fermionic and bosonic oscillator quanta. A detail study about choosing the HO basis is given in Sec. 3.2. The relativistic Lagrangian density for a nucleon–meson many-body systems is written as

$$\begin{aligned}\mathcal{L} = {} & \overline{\psi_i}\{i\gamma^\mu\partial_\mu - M\}\psi_i + \frac{1}{2}\partial^\mu\sigma\partial_\mu\sigma - \frac{1}{2}m_\sigma^2\sigma^2 - \frac{1}{3}g_2\sigma^3 - \frac{1}{4}g_3\sigma^4 - g_s\overline{\psi_i}\psi_i\sigma \\ & - \frac{1}{4}\Omega^{\mu\nu}\Omega_{\mu\nu} + \frac{1}{2}m_w^2V^\mu V_\mu - g_w\overline{\psi}_i\gamma^\mu\psi_iV_\mu - \frac{1}{4}\mathbf{B}^{\mu\nu}\cdot\mathbf{B}_{\mu\nu} + \frac{1}{2}m_\rho^2\mathbf{R}^\mu\cdot\mathbf{R}_\mu \\ & - g_\rho\overline{\psi}_i\gamma^\mu\boldsymbol{\tau}\psi_i\cdot\mathbf{R}^\mu - \frac{1}{4}F^{\mu\nu}F_{\mu\nu} - e\overline{\psi}_i\gamma^\mu\frac{(1-\tau_{3i})}{2}\psi_iA_\mu.\end{aligned} \tag{11}$$

Here, sigma meson field is denoted by σ, omega meson field by V_μ and rho meson field by $\mathbf{R}_u$ and A_μ denotes the electromagnetic field, which couples to the protons. The Dirac spinors are given by ψ for the nucleons, whose third component of isospin is denoted by τ_3 and g_s, g_2, g_3, g_ω, g_ρ are the coupling constants. The center

Table 1. The BE (MeV), rms radii (fm), quadrupole deformation parameter β_2 for Zr isotopes. The experimental results[38–40] are given for comparison.

	RMF(NL3*)						SHF(SLy4)						Expt.		
Nucleus	$r_{\rm ch}$	r_n	r_p	$r_{\rm rms}$	BE	β_2	$r_{\rm ch}$	r_n	r_p	$r_{\rm rms}$	BE	β_2	$r_{\rm ch}$	β_2	BE
^{80}Zr	4.282	4.123	4.207	4.165	664.5	−0.172	4.276	4.125	4.201	4.163	665.9	−0.154			
	4.274	4.112	4.198	4.155	665.9	0	4.262	4.108	4.186	4.147	669.2	0			669.9
	4.362	4.207	4.288	4.248	665.1	0.480	4.393	4.243	4.319	4.281	665.3	0.5001			
^{82}Zr	4.284	4.173	4.209	4.191	690.9	−0.191									
	4.272	4.158	4.197	4.177	691.7	0	4.269	4.151	4.193	4.172	694.4	0		0.367	694.5
	4.371	4.262	4.297	4.279	689.6	0.480	4.372	4.248	4.298	4.272	690.4	0.430			
^{94}Zr	4.324	4.453	4.249	4.367	809.8	−0.148	4.327	4.385	4.253	4.329	814.1	0	4.332	0.094	814.7
	4.326	4.452	4.251	4.368	809.4	0.163									
^{96}Zr	4.355	4.521	4.281	4.423	822.9	−0.191	4.344	4.432	4.269	4.365	826.8	0			
	4.368	4.520	4.294	4.427	823.2	0.240							4.351	0.08	829
^{98}Zr	4.381	4.585	4.307	4.473	835.4	−0.215	4.403	4.506	4.330	4.435	838.4	−0.196	4.401		840.9
	4.501	4.676	4.429	4.577	836	0.497									
^{100}Zr	4.400	4.639	4.327	4.517	846.9	−0.217	4.427	4.555	4.354	4.476	849.4	−0.210			
	4.487	4.690	4.415	4.582	847.7	0.445	4.512	4.612	4.441	4.545	849.7	0.421	4.49	0.355	852.2
^{102}Zr	4.416	4.687	4.343	4.555	858	−0.206	4.449	4.599	4.376	4.513	859.7	−0.215			
	4.496	4.732	4.424	4.614	858.3	0.430	4.536	4.654	4.465	4.581	860.5	0.429	4.53	0.427	863.6
^{104}Zr	4.436	4.735	4.363	4.595	868.7	−0.207	4.469	4.640	4.397	4.548	869.6	−0.219			873.8
	4.512	4.780	4.441	4.652	867.9	0.424	4.557	4.696	4.486	4.617	870.2	0.430			
^{106}Zr	4.461	4.783	4.389	4.639	878.5	−0.226	4.490	4.68	4.418	4.583	879.2	−0.223			883.2
	4.534	4.825	4.463	4.691	877.6	0.420	4.574	4.734	4.503	4.648	879.3	0.421			
^{108}Zr	4.483	4.829	4.411	4.679	886.8	−0.232	4.509	4.717	4.437	4.616	887.5	−0.226			
	4.439	4.816	4.366	4.654	886.5	0	4.463	4.697	4.391	4.586	885.2	0			891.7
	4.556	4.873	4.485	4.733	886.8	0.420	4.592	4.769	4.522	4.679	887.6	0.414			
^{110}Zr	4.487	4.865	4.415	4.707	894.3	−0.190	4.521	4.749	4.45	4.642	894.3	−0.210			
	4.454	4.864	4.381	4.964	896.2	0	4.48	4.733	4.408	4.617	893.9	0			899.5
	4.595	4.955	4.525	4.803	893.9	0.473	4.621	4.824	4.551	4.727	894.4	0.437			
^{112}Zr	4.500	4.904	4.429	4.740	901.9	−0.171	4.53	4.775	4.459	4.664	901.1	−0.176			
	4.469	4.903	4.397	4.729	902.7	0	4.496	4.765	4.424	4.646	901.1	0			906.5
	4.620	5.001	4.550	4.845	900.5	0.480	4.645	4.874	4.576	4.77	900.9	0.453			

of mass (c.m.) motion energy correction is estimated by the HO approximation $E_{\text{c.m.}} = \frac{3}{4}(41A^{-1/3})$. From the resulting proton and neutron quadrupole moments, the quadrupole deformation parameter β_2 is defined as

$$Q = Q_n + Q_p = \sqrt{\frac{16\pi}{5}}\left(\frac{3}{4\pi}AR_0^2\beta_2\right), \tag{12}$$

with $R_0 = 1.2A^{1/3}$ (fm), and the root-mean-square (rms) matter radius are given as

$$\langle r_m^2\rangle = \frac{1}{A}\int \rho(r_\perp, z)r^2 d\tau, \tag{13}$$

where A is the mass number and $\rho(r_\perp, z)$ is the deformed density. The total binding energy (BE) and other observables are also obtained by using the standard relations.[20]

3.1. *Pairing correlations in RMF formalism*

The pairing correlation plays an important role in open shell nuclei to describe the ground state properties, like BE, charge radius, single-particle energy levels and deformations. The relativistic Lagrangian contains only terms like $\psi^\dagger\psi$, and no terms of the form $\psi^\dagger\psi^\dagger$ at the mean-field level. The inclusion of the pairing correlation of the form $\psi\psi$ and two-body interaction $\psi^\dagger\psi^\dagger\psi\psi$ in the Lagrangian violates the particle number conservation.[28] We have used the pairing correlation externally in the RMF model. In our calculation, the constant gap BCS-approach takes care the pairing correlation for open shell nuclei. The general expression for pairing energy in terms of occupation probabilities v_i^2 and $u_i^2 = 1 - v_i^2$ is written as[28,29]:

$$E_{\text{pair}} = -G\left[\sum_{i>0} u_i v_i\right]^2, \tag{14}$$

with G = pairing force constant. The variational approach with respect to v_i^2 gives the BCS equation[29]:

$$2\epsilon_i u_i v_i - \triangle(u_i^2 - v_i^2) = 0, \tag{15}$$

with $\triangle = G\sum_{i>0} u_i v_i$.

The occupation number is defined as

$$n_i = v_i^2 = \frac{1}{2}\left[1 - \frac{\epsilon_i - \lambda}{\sqrt{(\epsilon_i - \lambda)^2 + \triangle^2}}\right]. \tag{16}$$

The values $\triangle$ for the nucleons (neutron and proton) is taken from the phenomenological formulae of Madland and Nix[27]:

$$\triangle_n = \frac{r}{N^{1/3}}\exp(-sI - tI^2), \quad \triangle_p = \frac{r}{Z^{1/3}}\exp(sI - tI^2), \tag{17}$$

where, $I = (N - Z)/A$, $r = 5.73\,\text{MeV}$, $s = 0.117$ and $t = 7.96$.

The chemical potentials λ_n and λ_p are determined by the particle numbers for neutrons and protons. Finally, the pairing energy is computed as

$$E_{\text{pair}} = -\triangle \sum_{i>0} u_i v_i. \tag{18}$$

For a particular value of $\triangle$ and G, the pairing energy E_{pair} diverges, if it is extended to an infinite configuration space. In fact, in all realistic calculations with finite range forces, the contribution of states of large momenta above the Fermi surface (for a particular nucleus) to $\triangle$ decreases with energy. Therefore, we have used a pairing window, where the equations are extended up to the level $|\epsilon_i - \lambda| \leq 2(41A^{-1/3})$ as a function of the single-particle energy. The factor two has been determined so as to reproduce the pairing correlation energy for neutrons in ^{118}Sn using Gogny force.[22,28,30] It is to be noted that recently Karatzikos *et al.*[31] has shown that if one uses the constant pairing window which is adjusted for one state at particular deformation then it may lead to errors at different energy solution (different state solution). However, we have not taken this problem into account in our calculations, as we have adjusted to reproduce the pairing as a whole for ^{118}Sn nucleus.

3.2. *Selection of basis space*

After getting the set of coupled mean-field equations for both nucleons and mesons, we need to solve these equations numerically by expanding the wave functions (potentials) in the deformed HO basis and solve the equations iteratively. For the exotic (drip line) nuclei, a large model space is required to get a proper convergence solution of the system. We have used the HO quanta $N_F = N_B = 12$, where N_F for fermionic and N_B for bosonic fields. The convergence of the results, like BE, rms matter radius (r_{rms}) and quadrupole deformation parameter (β_2) with the HO basis are tested and the obtained values are shown in Fig. 1. The convergence test is done as a function of HO basis for normal and larger deformations ($\beta_0 = 0.6$). An increase in basis quanta from 12 to 14, the increment in energy is $\sim$0.21 MeV which is near the accuracy of the present RMF model. Also, to be noted that a further increase in the model space, the convergence time increases dramatically. Thus, an optimum values of $N_F = N_B$ need to be chosen, and can be seen in Fig. 1 that this values of $N_F = N_B \geq 12$ is a suitable choice.

To study the convergence of the solutions in both RMF (NL3*) and SHF (SLy4) formalisms, we have calculated the binding energy and corresponding quadrupole moment with different basis deformation for the quadrupole moments. It is found that the calculated quadrupole deformation parameter β_2 is independent of the basis deformation β_0. Both the formalisms estimate reasonable results except for the spherical solution obtained with an basis deformation $\beta_0 = 0.03$. Due to this odd behavior of SHF(SLy4) at the spherical solution, we ignore it for further analysis. We perform the calculations for ^{82,100,102,104}Zr isotopes and the results are given in Table 3. It is to be noted that from the potential energy surface curve as well as from the analysis of basis deformation, we get a spherical solution for lighter

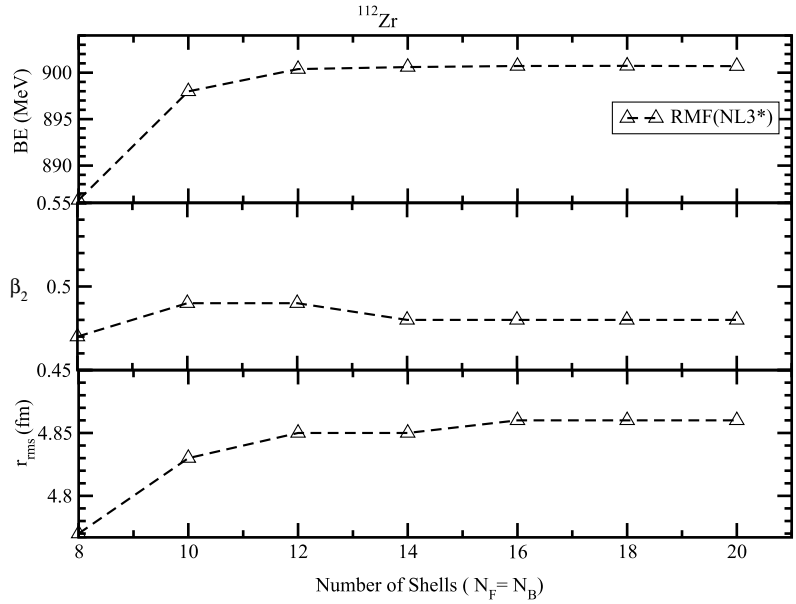

Fig. 1. (Color online) The calculated BE, rms matter radius ($r_{\rm rms}$) and quadrupole deformation parameter (β_2) with Bosonic and fermionic basis. The minima of the solution obtained with $N_F = N_B = 8$–20 are shown. One can see from the figure that the results are almost similar with each other for $N_F = N_B = 12$ or more showing the stability of the solution for $N_F = N_B = 12$.

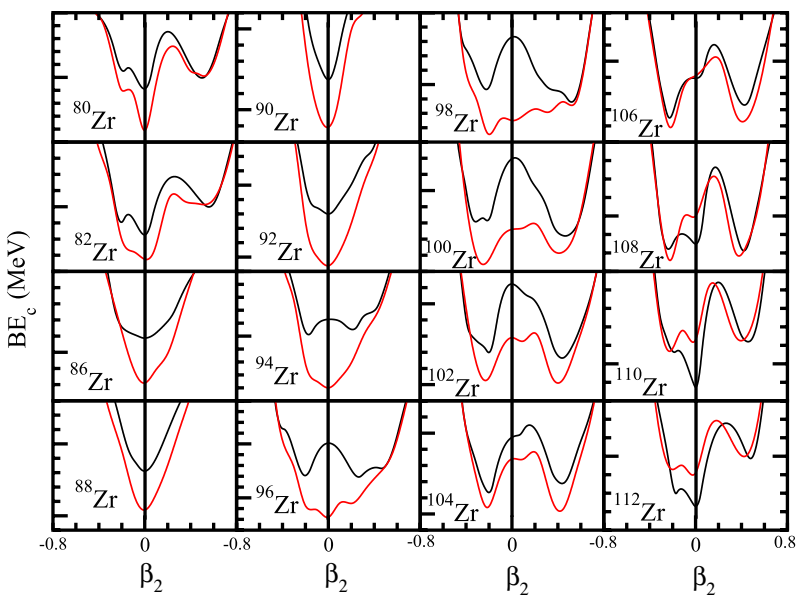

Fig. 2. (Color online) The potential energy surface for the Zr isotopes for NL3* (black line) and SLy4 (red line) force parameter.

isotopes of Zr, such as $^{82-92}$Zr. However, the zero deformation is not stable for heavier masses of Zr upto $A = 106$. Again, beyond $A = 108$, the solutions with zero deformation get stabilized with increase in mass number (see Potential Energy Surface (PES) curve Fig. 2).

4. Calculations and Results

We have used the nonconstraint calculation in both the RMF and SHF formalisms. For this, first we have put some basis deformation parameter and let the system go to find out the minimum energy state in local region corresponding to the basis deformation i.e., β_0. Here, we have put the three assumption values for each nucleus ($\beta_0 = 0.001, \pm 0.3$). In most of the cases, the obtained quadrupole deformation parameter β_2 of the nucleus may be different from the basis deformation β_0. Both the SHF and RMF formalisms predict satisfactory results for binding energy, rms radius and quadrupole deformation parameter β_2, not only for nuclei in stability line, but also for drip lines nuclei. In this work, we have analyzed the structure of proton and neutron-rich Zr nuclei and studied two important phenomena such as (i) shape coexistence and (ii) parity doublet for some specific Zr isotopes. Also, the matter radius r_m, quadrupole deformation parameter β_2 and ground state binding energy are estimated from proton to neutron driplines. The calculated results are given in Table 2 and the shape coexistence and parity doublets are shown in Figs. 3–6.

4.1. *PES*

Except few isotopes, a large number of nuclei in the mass table are found to be deformed in their ground state configuration. For the calculation of the ground state properties one should include the deformation into the formalisms. It may possible that some nuclei have almost same energy with different shape configurations (spherical, prolate or oblate). This type of states are known as shape coexistence. To get the solution with different deformations one should perform the constraint calculation as a function of quadrupole deformation parameter with various constraint BE (BE$_c$). For constraint calculation, we minimize $\langle H' \rangle$ instead of $\langle H \rangle$ which are related to each other by the following relation[32–36]:

$$H' = H - \lambda Q, \quad \text{with } Q = r^2 Y_{20}(\theta, \phi), \tag{19}$$

where, λ is the Lagrange multiplier which is fixed by the constraint $\langle Q \rangle_\lambda = Q_0$. In the present work, we have done the constraint calculation for Zr isotopes for both the parameter sets (NL3* and SLy4) and the obtained results are shown in Fig. 2. Apart from a few exceptions, in general, we get qualitatively similar results in both the formalisms. For example, in SHF(SLy4) case, the three minima of ^{110}Zr are located at $\beta_2 = -0.210$, 0 and 0.437 respectively. Similar situation can be found for ^{108,112}Zr nuclei. The ground state potential energy surfaces allow us to determine the equilibrium shapes (the lowest minimum). It is worthy to mention that the

Table 2. The BE (MeV), quadrupole deformation parameter β_2 and basis deformation parameter β_0 for Zr isotopes.

	RMF(NL3*)		SHF(SLy4)				RMF(NL3*)		SHF(SLy4)		
Nucleus	BE	β_2	BE	β_2	β_0	Nucleus	BE	β_2	BE	β_2	β_0
^{82}Zr	691	−0.194	691.8	−0.182	−0.6	^{102}Zr	858.1	−0.208	859.7	−0.216	−0.6
	691	−0.192	691.8	−0.178	−0.5		858.1	−0.206	859.7	−0.216	−0.5
	690.9	−0.191	691.8	−0.146	−0.4		858	−0.205	859.7	−0.215	−0.4
	690.9	−0.191	691.8	−0.164	−0.3		858	−0.206	859.7	−0.215	−0.3
	690.8	−0.190	692.2	−0.117	−0.2		858	−0.206	859.7	−0.215	−0.2
	691.7	0	692.5	−0.103	−0.1		858	−0.207	859.7	−0.215	−0.1
	691.7	0	694.4	0	0.03		858.2	0.419	857.3	0	0.0.3
	691.7	0	690	0.461	0.1		858.3	0.426	860.5	0.429	0.1
	691.7	0	690	0.477	0.2		858.3	0.429	860.5	0.428	0.2
	689.4	0.493	690	0.493	0.3		858.2	0.429	860.6	0.428	0.3
	689.4	0.481	690	0.496	0.4		858.2	0.429	860.6	0.428	0.4
	689.4	0.473	690	0.484	0.5		858.3	0.430	860.5	0.429	0.5
	689.6	0.480	690.4	0.430	0.6		858.1	0.428	860.5	0.429	0.6
^{100}Zr	846.9	−0.218	849.4	−0.212	−0.6	^{104}Zr	868.7	−0.208	869.6	−0.220	−0.6
	846.9	−0.217	849.4	−0.211	−0.5		868.7	−0.206	869.6	−0.219	−0.5
	846.9	−0.216	849.4	−0.211	−0.4		868.7	−0.206	869.6	−0.219	−0.4
	846.9	−0.217	849.4	−0.210	−0.3		868.7	−0.207	869.6	−0.219	−0.3
	846.8	−0.218	849.4	−0.210	−0.2		868.6	−0.207	869.7	−0.219	−0.2
	846.8	−0.218	849.5	−0.210	−0.1		868.6	−0.208	869.7	−0.219	−0.1
	847.6	0.423	847.5	0	0.03		865.2	0	866.8	0	0.03
	847.7	0.440	849.7	0.423	0.1		865.1	0.035	870.3	0.430	0.1
	847.7	0.449	849.7	0.422	0.2		868	0.424	870.3	0.430	0.2
	847.7	0.445	849.7	0.421	0.3		868	0.424	870.3	0.430	0.3
	847.6	0.440	849.7	0.422	0.4		867.9	0.424	870.3	0.430	0.4
	847.6	0.436	849.7	0.423	0.5		867.9	0.423	870.3	0.430	0.5
	847.6	0.433	849.6	0.422	0.6		867.9	0.424	870.2	0.430	0.6

Table 3. The pairing gap, effective strength and pairing energy for Zr isotopes.

	RMF(NL3*)			SHF(SLy4)				
Nucleus	$\triangle_n$	$\triangle_p$	E_{pair}	G_n	G_p	$\triangle_n$	$\triangle_p$	E_{pair}
^{80}Zr	1.673	1.673	18.995	−0.162	−0.158	0.158	0.143	4.578
^{82}Zr	1.633	1.669	19.078	−0.149	−0.157	0.217	0.142	5.911
^{94}Zr	1.242	1.422	15.188	−0.126	−0.145	0.169	0.124	4.485
^{96}Zr	1.170	1.361	13.882	−0.125	−0.144	0.183	0.118	4.889
^{98}Zr	1.100	1.300	11.999	−0.125	−0.141	0.194	0.135	5.44
^{100}Zr	1.031	1.238	11.411	−0.121	−0.140	0.222	0.133	6.156
^{102}Zr	0.966	1.176	10.767	−0.118	−0.138	0.251	0.131	6.695
^{104}Zr	0.903	1.115	9.886	−0.116	−0.134	0.163	0.103	4.183
^{106}Zr	0.844	1.056	8.840	−0.114	−0.133	0.158	0.095	3.948
^{108}Zr	0.787	0.999	7.741	−0.112	−0.132	0.139	0.091	3.517
^{110}Zr	0.735	0.944	6.971	−0.109	−0.133	0.143	0.084	3.468
^{112}Zr	0.685	0.892	6.959	−0.106	−0.132	0.124	0.082	3.058

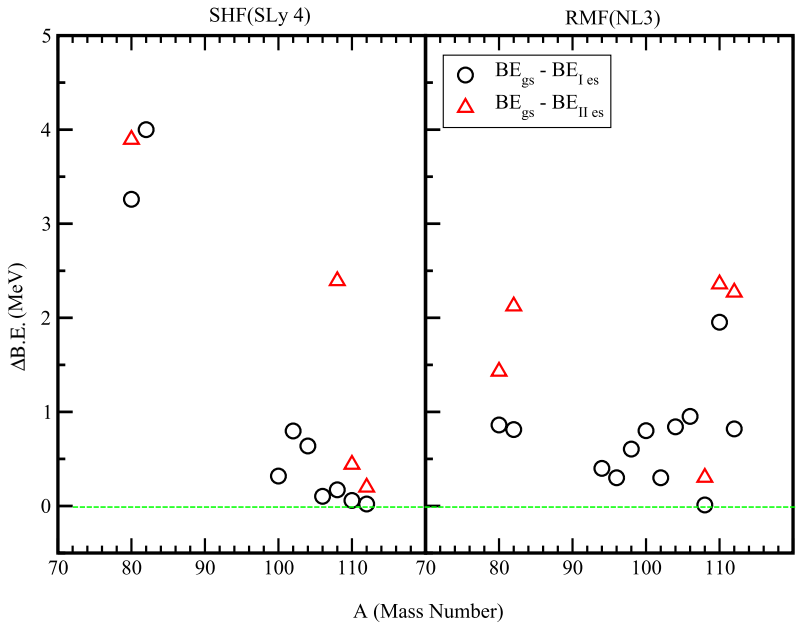

Fig. 3. (Color online) The ground state BE difference from first and second intrinsic excited states for Zr isotopes. The zero reference point shown by the dashed horizontal line.

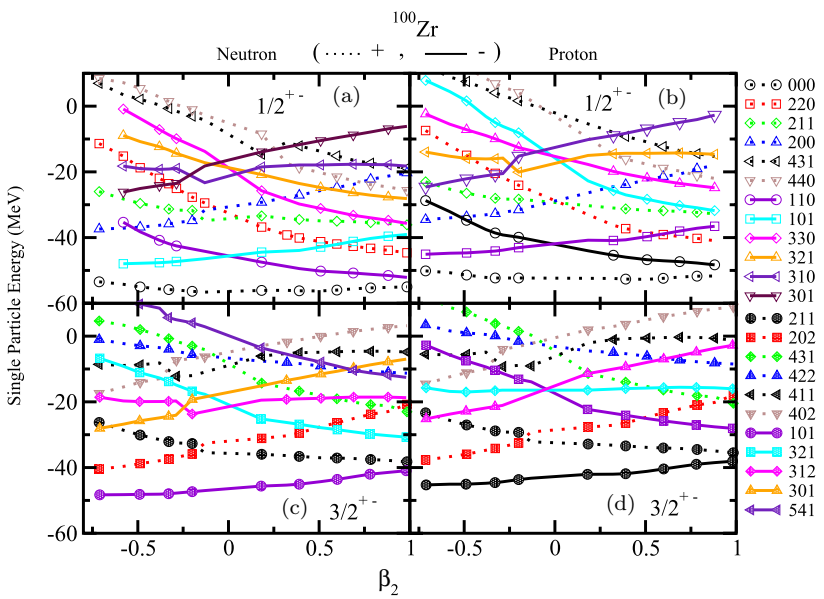

Fig. 4. (Color online) Some selected single-particle energy level evolution with deformation parameter β_2 for relativistic model by using NL3* parameter set. (a) 1/2+− Single-particle levels for the neutron, (b) 1/2+− Single-particle levels for proton, (c) 3/2+− Single-particle levels for neutron, and (d) 3/2+− Single-particle levels for proton. The positive parity (+) level is given by dotted line and negative parity levels (−) level is given by solid line.

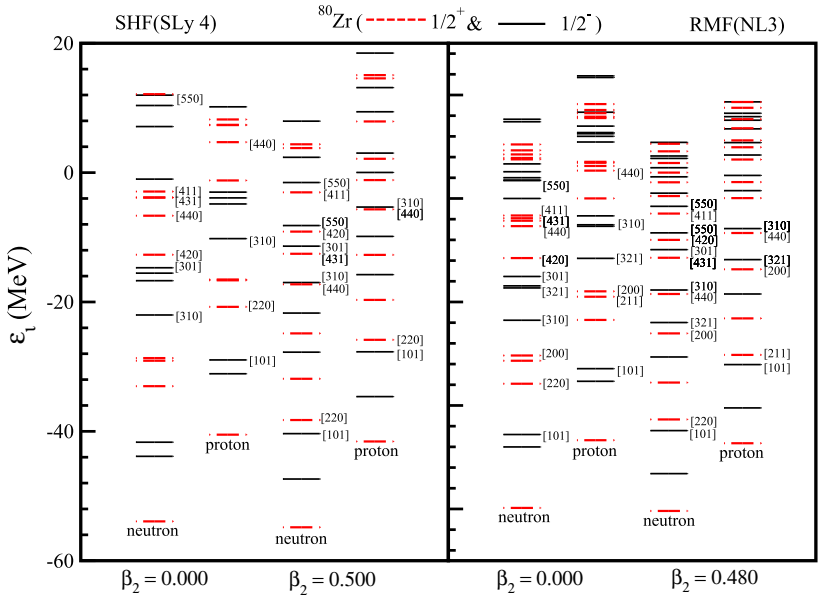

Fig. 5. (Color online) Single-particle levels for ^{80}Zr in normal and large deformed states. The single-particle levels are denoted by the Nilsson indices $[N, n_z, \Lambda]\Omega^{\pi}$.

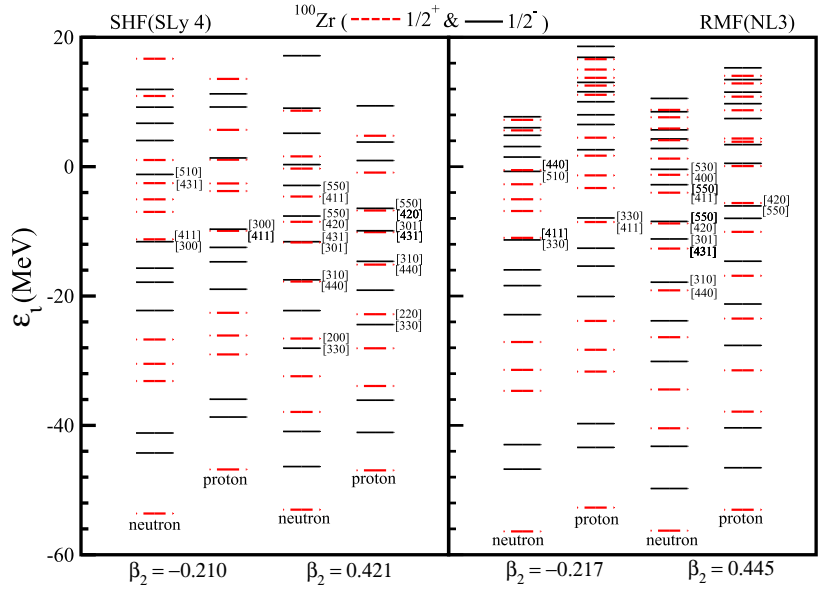

Fig. 6. (Color online) Single-particle levels for ^{100}Zr isotopes in oblate and large deformed states.

minima near zero is not well developed, and may be considered as an isomeric state. Thus, we get three solutions in such nuclei consistent with the earlier report of Schunck *et al.*[37] In addition to this, we also notice shallow regions in the PES with several flat minima for ^{96,98,100,102}Zr. This fluctuation may be due to the use of mean-field models and one needs a theory beyond mean-field to over come such fluctuations. For example, the generator coordinate method or random phase approximation could be some improved formalisms to take care of such effects.

4.2. *BE and shape coexistence*

The nuclear BE is a physical quantity, which is precisely measured experimentally and it is responsible for nuclear stability and structure of nuclei. The maximum BE corresponds to the ground state and all other solutions are intrinsic excited states of a nucleus. These are not necessarily the lowest excitations, there could be rotational excitations below their first excited state, which is beyond the scope of our present calculations and needs further analysis. The BE for Zr isotopes obtained by SHF(SLy4) and RMF(NL3*) calculations are depicted in Table 2 and the results compared with experimental data,[38–40] wherever available. From the ground and excited intrinsic states BEs, we have measured their difference $\triangle$BE = BE(gs) − BE(es) and examined the shape coexistence phenomena. When we find a small value of $\triangle$BE, then we termed it as a case of shape coexistence (degenerate solutions with different quadrupole deformations). For shape coexistence, there is a good possibility of the nucleus being in either shapes.

The BE difference between the ground and first and second intrinsic excited states are shown in Fig. 3 for Zr isotopes. The solid line is the zero reference label, which marks the shape coexistence line. The points which are on the line designated as perfectly shape coexistent nuclei. The shape coexistence in $A = 80$ mass region of nuclei using RMF formalism have been reported in Refs. 4, 28 and 41. Here, it is shown that the neutron-deficient nuclei in this mass region possess spherical and large deformed structures. In the present work, we would like to show that not only the neutron-deficient Zr isotopes have shape coexistence, but also other normal and neutron-rich Zr isotopes have low-lying large deformed configuration including the normal/spherical shape. Sometimes it so happens that the large deformed solution becomes the ground state (^{98}Zr, $\beta_2 = 0.497$ in RMF) as shown in the Table 2. The nuclei with shape coexistence shows the transition between the spherical to oblate and again from oblate to prolate due to minimum energy barrier between the shape coexistence states. There are some isotopes, i.e., ^{108}Zr (in RMF) and ^{110,112}Zr (in SHF), which have ΔBE ≤ 1 MeV for both cases like first and second intrinsic excited states. This type of shape coexistence is called triple shape coexistence.[9] If we see the ΔBE for ^{108}Zr in Fig. 3, its excited state has almost same energy with its ground state, leading to the phenomenon of shape coexistence. These type of nuclei show the shape coexistence in their excited state and performed the shape change/fluctuation in application of a small energy (≤ 1 MeV). The shape coexistence is very important

in the reaction study, because surface density distribution plays a crucial role in the cross-section and it will change by applying small perturbation in energy. Some isotopes of Zr have been predicted to be triaxial ($\gamma \neq 0$)[42] in shape, which is one more degree of freedom in shape orientation. The study of this phenomenon is beyond the scope of this work, as we have used the axially symmetric formalism for the deformed nuclei.

In the present work, we have compared both results of SLy4 and NL3* with the experimental data in Table 2. Analyzing Fig. 3 and the BE results of Table 2, it is clear that the prediction of RMF(NL3) and SHF(SLy4) are qualitatively almost similar. Again, comparing the results with experimental data, the SLy4 parameter set reproduce the data similar or even better than NL3* set of the RMF formalism. In general, both the SHF and RMF have tremendous predictive power upto an acceptable extend of accuracy and the results can be used to most part of the mass Table. Also, it is worthy to mention that all models have some limitations and there are every possibilities for their improvements.

4.3. *Evolution of single-particle energy with deformation*

In this section, we have calculated the single-particle energy of some selected Nilsson orbits with different values of deformation parameter β_2 by the constraint calculation. The results are given in Fig. 4, where positive parity orbits shown by dotted and negative parity by solid lines for ^{100}Zr isotope. The single-particle energy for neutron is given in Fig. 4(a) and proton single-particle energy in Fig. 4(b). The lower level like $\frac{1}{2}^+[000]$ is very less affected by the variation of the deformation in both neutron and proton cases as shown in Figs. 4(a) and 4(b). But as we increase the energy of the levels, variation of single-particle energy also increases with the deformation parameter as shown in figure. We have plotted similar curve for $\frac{3}{2}^\pm$ orbits for the same nucleus ^{100}Zr and the results obtained are given in Figs. 4(c) and 4(d) for neutron and proton, respectively. The evolution of single-particle energy levels with deformation parameters is of similar nature as $\frac{1}{2}^\pm$ orbits. We repeat the calculation in nonrelativistic SHF model and obtained almost similar trend of levels, so we are not presenting the SHF results. The single-particle energies evolved with the deformation parameter and opposite parity orbits come closer with deformation. A detailed study is done in the following section, where we will discuss about the parity doublets in the orbits at large deformation.

4.4. *Large deformed configuration and parity doublet*

The parity doublet is an interesting configuration for the large deformed state of a nucleus. Recently, it has been reported by Singh *et al.*[1] and they have shown that there exist a parity doublet in the large deformed configuration for light mass nuclei. In the present calculations, we have extended the investigation to relatively heavier mass region of the periodic chart. In this case, we have focused our study on Zr isotopes, where shape coexistence is an usual phenomenon. In most of the cases

of Zr isotopes, we get a spherical or a normal deformed solution along with a large deformed state both in the RMF(NL3*) and SHF(SLy4) calculations. The evolution of single-particle energy with deformation parameter β_2 for some selected nuclei are depicted in Figs. 5 and 6. The parity doublets are marked by their asymptotic quantum number $[N, n_z, \Lambda]$, where N is principle quantum number, n_z is number of nodes of the wave function in the z-direction (the number of times the radial wave function crosses zero). Larger n_z values corresponds to wave function more extended in the z-direction which means lower energy orbits, Λ is the projection of the orbital angular momentum on to the z-axis. As in light mass nuclei,[1] in case of Zr isotopes also, the deformation-driving $\Omega^\pi = \frac{1}{2}^-$ orbits come down in energy in large deformed solutions from the shell above, in contrast to the normal deformed solutions. For each nucleus, we have compared the normal/spherical deformed and the large deformed configurations single-particle energy orbits and analyzed the parity doublets states and some of them are given in this work. The occurrence of approximate $\frac{1}{2}^+$, $\frac{1}{2}^-$ parity doublets (degeneracy of $\Omega^\pi = \frac{1}{2}^+$, $\frac{1}{2}^-$ states) for the large deformed solutions are clearly seen in Figs. 5 and 6, where excited large deformed configurations for ^{80}Zr and ^{100}Zr are given. As shown in Fig. 5, the single-particle levels for spherical shape for opposite parity are well-separated from each other, but become closer with deformation suggesting parity doublets in the system. For example, in the case of ^{80}Zr, if we have plotted the single-particle energy levels for neutron, then the energy levels $[310]\frac{1}{2}^-$ and $[440]\frac{1}{2}^+$ are far from each other ($\sim$18.28 MeV in RMF), but becomes almost degenerate ($\sim$1.28 MeV) at large-deformation ($\beta_2 = 0.480$). Same behavior we have found in the single-particle orbits $[440]\frac{1}{2}^+$ and $[310]\frac{1}{2}^-$ of proton intrinsic single particles, i.e., in normal deformation, these two levels are separated from each other by 16.8 MeV, but in large deformed case ($\beta_2 = 0.480$), it becomes closer ($\sim$0.5 MeV). Qualitatively, the same behavior appears in the SHF(SLy4) results also (left panel of the Figs. 5 and 6). In Fig. 6, for ^{100}Zr we have given the large deformed orbits for prolate and oblate cases both for RMF(NL3*) and SHF(SLy4) models. Here also, we get the parity doublet in oblate and prolate shapes, which implies that parity doublets are driving by the deformation and it will occur at the large deformation. Some parity doublet orbits are shown by Nilsson representation $[N, n_z, \Lambda]$ in Fig. 6. On close inspection of Fig. 6, then in the oblate level of neutron, we get several parity doublets like ([411] [330]), ([440] [510]) and for proton ([330] [411]). For prolate case, the neutron parity doublet orbits ([530] [400]), ([550] [420]), ([301] [431]), ([310] [440]) etc., similarly for the proton case.

5. Summary and Conclusions

We have calculated the ground and low-lying excited state properties, like BE and quadrupole deformation parameter β_2 using RMF(NL3*) and SHF(SLy4) formalisms for Zr isotopes near the drip line regions. In general, both the RMF and SHF models have predicted very good results throughout the isotropic chain. We

get the double and triple shape coexistence from our analysis in some Zr isotopes, which is consistent with the earlier data. The present prediction of parity doublet may be a challenge for the experimentalist to look for such configuration states. In general, we find large deformed solutions for the neutron-drip nuclei, which agree with the experimental measurements. In the calculations, a large number of low-lying intrinsic large deformed excited states are predicted in many of the isotopes, which shows the parity doublet near the Fermi levels. The parity doublet levels are nearly degenerate in excited states which can make two bands of different parity promoting two particles from reference frame to these degenerate opposite parity levels. It may solve the problem of existence of the twin bands and quantization of alignments of shapes. This analysis will help us to understand the intrinsic excited states of the Zr and other similar isotopes. In this respect, some more calculations are required to build a general idea about the omega parity doublets.

References

1. S. K. Singh, C. R. Praharaj and S. K. Patra, *Cent. Eur. J. Phys.* **12** (2014) 42.
2. C. R. Praharaj, *Int. Workshop Nucl. Many-Body Theor. for 21st Century* (University of Washington, Seattle, 2007).
3. K. Sugawara-Tanabe and A. Arima, *Phys. Lett. B* **317** (1993) 1.
4. J. P. Maharana, Y. K. Gambhir, J. A. Sheikh and P. Ring, *Phys. Rev. C* **46** (1992) R1163.
5. S. K. Patra and C. R. Praharaj, *Phys. Rev. C* **47** (1993) 2978.
6. F. Sarazin *et al.*, *Phys. Rev. Lett.* **84** (2000) 5062.
7. J. L. Egido, L. M. Robledo and R. R. Rodriguez-Guzman, *Phys. Rev. Lett.* **93** (2004) 282502.
8. S. K. Singh, M. Ikram and S. K. Patra, *Int. J. Mod. Phys. E* **22** (2013) 1350001.
9. A. Petrovici, *Phys. Rev. C* **85** (2012) 034337.
10. M. V. Stoitsov, J. Dobaczewski, W. Nazarewicz, S. Pittel and D. J. Dean, *Phys. Rev. C* **68** (2003) 054312.
11. E. Chabanat, P. Bonche, P. Haensel, J. Meyer and R. Schaeffer, *Nucl. Phys. A* **635** (1998) 231.
12. M. V. Stoitsov, J. Dobaczewski, W. Nazarewicz and P. Ring, *Comput. Phys. Commun.* **167** (2005) 43.
13. H. J. Lipkin, *Ann. Phys.* **9** (1960) 272.
14. H. Flocard and N. Onishi, *Ann. Phys.* **254** (1997) 275.
15. P. Ring and P. Schuck, *The Nuclear Many-Body Problem* (Springer-Verlag, Berlin, 1980).
16. P. Ring, Y. K. Gambhir and G. A. Lalazissis, *Comput. Phys. Commun.* **105** (1997) 77.
17. M. Bender, P.-H. Heenen and P. G. Reinhard, *Rev. Mod. Phys.* **75** (2003) 121.
18. E. Perlińska, S. G. Rohoziński, J. Dobaczewski and W. Nazarewicz, *Phys. Rev. C* **69** (2004) 014316.
19. K. Bennaceur and J. Dobaczewski, *Comput. Phys. Commun.* **168** (2005) 96.
20. S. K. Patra and C. R. Praharaj, *Phys. Rev. C* **44** (1991) 2552.
21. J. D. Walecka, *Ann. Phys.* **83** (1974) 491.
22. B. D. Serot and J. D. Walecka, *Adv. Nucl. Phys.* **16** (1986) 1.
23. C. J. Horowitz and B. D. Serot, *Nucl. Phys. A* **368** (1981) 503.
24. J. Boguta and A. R. Bodmer, *Nucl. Phys. A* **292** (1977) 413.

25. C. E. Price and G. E. Walker, *Phys. Rev. C* **36** (1987) 354.
26. G. A. Lalazissis, S. Karatzikos, R. Fossion, D. P. Arteaga, A. V. Afanasjev and P. Ring, *Phys. Lett. B* **671** (2009) 36.
27. D. G. Madland and J. R. Nix, *Nucl. Phys. A* **476** (1981) 1.
28. S. K. Patra, *Phys. Rev. C* **48** (1993) 1449.
29. M. A. Preston and R. K. Bhaduri, *Structure of the Nucleus* (Addison-Wesley, 1982), Ch. 8, p. 309.
30. J. Decharg and D. Gogny, *Phys. Rev. C* **21** (1980) 1568.
31. S. Karatzikos, A. V. Afanasjev, G. A. Lalazissis and P. Ring, *Phys. Lett. B* **689** (2010) 72.
32. S. K. Patra, F. H. Bhat, R. N. Panda, P. Arumugam and R. K. Gupta, *Phys. Rev. C* **79** (2009) 044303.
33. H. Flocard, P. Quentin and D. Vautherin, *Phys. Lett. B* **46** (1973) 304.
34. W. Koepf and P. Ring, *Phys. Lett. B* **212** (1988) 397.
35. J. Fink, V. Blum, P.-G. Reinhard, J. A. Maruhn and W. Greiner, *Phys. Lett. B* **218** (1989) 277.
36. D. Hirata, H. Toki, I. Tanihata and P. Ring, *Phys. Lett. B* **314** (1993) 168.
37. N. Schunck, J. Dudek, A. Góźdź, and P. H. Regan, *Phys. Rev. C* **69** (2004) 061305(R).
38. S. Raman, C. W. Nestor, Jr. and P. Tikkanen, *At. Data Nucl. Data Tables* **78** (2001) 1.
39. M. Wang, G. Audi, A. H. Wapstra, F. G. Kondev, M. Mac-Cormick, X. Xu and B. Pfeiffer, *Chin. Phys. C* **36** (2012) 1603.
40. I. Angeli and K. P. Marinova, *At. Data Nucl. Data Tables* **99** (2013) 69.
41. A. Chakraborty *et al.*, *Phys. Rev. Lett.* **110** (2013) 022504.
42. T. R. Rodríguez and J. L. Egido, arXiv:1109.6511v1 [nucl-th].